

Combined low-Reynolds-number $k - \epsilon$ model for recirculating flows

CHARLES CHELEM¹, MARCEL OBOUNOU², ELKANA PEMHA¹, CLEMENT TCHAWOUA²

1. ZARM - Center of Applied Space Technology and Microgravity, Universität Bremen, Am Fallturm, 28359 Bremen, GERMANY
2. Faculty of sciences, Department of Physics, University of Yaoundé 1 Po Box 812 Yaoundé, Cameroon Email: c_m_chelem@yahoo.fr

Abstract: The aim of this work is the numerical simulation of turbulent flow with separation and reattachments. In The present paper, the low-Reynolds-number (LRN) $k - \epsilon$ turbulence is combined with standard $k - \epsilon$ turbulence model using two different formulations for predicting the length of the reattachment point in the separated flow. The developed model is validated with Jovic and Driver (1994) backward facing step problem before being applied to the problem of recirculating flow over repeated square ribs. Performance of the models is investigated and compared with available experimental data, Direct Numerical Data and numerical results using other turbulence models. It is seen that the models provide good predictions of secondary flows beyond the step.

Keywords: Turbulence, Low-Reynolds Number, $k - \epsilon$ model, Recirculating flow, Length of reattachment, Secondary flows, Finite volumes method.

1. INTRODUCTION

Turbulence models are widely used for simulating complex heat transfer and flow phenomena in many engineering applications because of their simplicity and effectiveness. The most popular form is the one proposed by Launder and Spalding [1], the so called the standard $k - \epsilon$ model (High-Reynolds model). However, the disadvantage of the standard $k - \epsilon$ model with wall functions is the inability to predict accurate near-wall flow characteristics. The lack of universality of the wall functions has been frequently criticized [2]. To solve the near-wall effect, a number of Low-Reynolds Number models (LRN model) have been developed [3]. The first LRN $k - \epsilon$ model was developed by Jones and Lander [4] and subsequently modified by many researchers. To get a better understanding of the near-wall effect, many LRN models were developed based on the High-Reynolds (High-

Re) $k - \epsilon$ model [5, 6, 7, 8]. Several concepts were also used to increase model accuracy. Menter [9] proposed a model to resolve the free stream dependency by blending the standard Wilcox model and the standard $k - \epsilon$ model. Combining the High-Re $k - \omega$ with the $k - \epsilon$ model, Menter [10] developed two new models and improved prediction of adverse pressure gradient flows. Bredberg and Davidson [11] presented a new-wall treatment for LRN turbulence model based on $k - \omega$ model that maintains accuracy in coarse mesh predictions. Wang and Mujundar [12] applied the Yap correction [13] to five characteristics of a two-dimensional turbulent slot jet. The predicted results in wall jet regions are in good agreement with the experimental data. Jia et al. [14] integrated the reformulated SSG model [15] based on the ω -equation and the SST model [10]. The new model was called SSG-SST model. Khuwaranyu and Putivisitak [16]

combined the LRN $k-\omega$ model with a Length Scale Correction (LSC) term for solving recirculating flow. The model gives superior results especially for the near-wall flow patterns.

The current work presents two new concept turbulence models, namely Blended LRN $k-\epsilon$ Model (BLM) and Mixed Eddy Viscosity Model (MEVM). The concept of the new model is based on a combination of accurate formulation of one of the Abid [17] LRN $k-\epsilon$ model in the near-wall region with the standard $k-\epsilon$ model (High-Re $k-\epsilon$ model) in the free stream region. The developed models are validated with available experimental data, DNS data and numerical results using other turbulence models.

In the present case, the flow undergoes an adverse pressure gradient: the pressure rises in the direction of flow, resulting in a separation of the boundary layer. The flow, if confined, catch up with flow channel at downstream, forming a recirculation zone. This recirculation zone results in a significant increase in drag. It is therefore important to understand the mechanisms of detachment and reattachment before designing industrial structures. Among the most frequently used geometries for the study of separated flows, are the backward-facing step [18] due to the relative simplicity of its geometry, the separation point located at the step, the difficulties related to possible oscillation of the latter and the existence of experimental results are avoided. More recently, Hattori et al. [19] conducted a direct numerical simulation (DNS) of a boundary layer which improved understanding of the turbulence phenomena in the boundary layer with several effects. They constructed a flow database to evaluate a turbulence model.

The Computational Fluid Dynamics (CFD) is a very powerful tool for the analysis of complex fluid flow engineering problems. It incorporates modeling of various flow effects, such as turbulence, heat and mass transfer. Concerning the turbulence models, vast majority of the CFD users stay within the Reynolds-Averaged

Navier-Stokes (RANS) formalism, deploying the two-equation eddy viscosity models. Indeed the knowledge of the parameters of the turbulence may help in understanding complicated phenomena such as erosion, sediment transport, turbidity currents, resistance and design of industrials structures, the behavior of pollutants or calculation of discharge points for wastewater. This study has been carried out on FLUENT software [20] version 6.3.26. The last paragraphs in this section present the details of the model implementation in case of commercial CFD package FLUENT [20]. The starting point for the implementation of the Hybrid LRN $k-\epsilon$ model and standard $k-\epsilon$ model into RANS-based CFD fluid flow solver is the generic transport equation of the standard form. For an arbitrary passive scalar ϕ (e.g. additional turbulent quantities or chemical species) this equation can be written as:

$$\frac{\partial \phi}{\partial t} + U_j \frac{\partial \phi}{\partial x_j} = \frac{\partial}{\partial x_j} \left[D_\phi \frac{\partial \phi}{\partial x_j} \right] + S_\phi$$

(1)

And by solving this equation in the course of the numerical simulation the additional passive scalars, which in FLUENT are called the User Defined Scalars (UDS), can be introduced into numerical simulation.

The generic transport equation of the standard form (1) consists of four terms: the local rate of change which is activated for the unsteady flow calculations only, the convection, the diffusion for which the diffusivity coefficient D_ϕ is to be defined, and finally the source term S_ϕ on the right hand side of Eq.(1). The k and ϵ source terms required for the LRN $k-\epsilon$ model implementation, are summarized in the table 1.

Table 1: sources terms for k and ϵ

| S_k | S_ϵ |
|---------------|--------------------------------------------------------------------------|
| P- ϵ | $\frac{k(f_1 C_{\epsilon 1} P - f_2 C_{\epsilon 2} \epsilon)}{\epsilon}$ |

It was found that all the methods using the standard $k-\epsilon$ model underpredicted the reattachment length as measured by experiment

[21]. These results indicate that a modification to the model is necessary. The activation of the Hybrid LRN $k-\epsilon$ model and standard $k-\epsilon$ model definition of the turbulent viscosity [22] is actually the key point in the implementation of this model, as all the turbulence effects are coming into play through the μ_t in the framework of eddy-viscosity turbulence modeling.

2. Mathematic Formulations

The Reynolds-averaging principle is applied to the Navier-Stokes equations. After performing the averaging, the continuity and momentum equations can be written as follows:

$$\frac{\partial \rho}{\partial t} + \frac{\partial(\rho \bar{u}_i)}{\partial x_i} = 0 \tag{2}$$

(3)

Where $\overline{\rho u_i' u_j'}$ are the Reynolds stresses ($R_{ij} = -\overline{\rho u_i' u_j'}$).

2.1 Description of Turbulence Models

All of the two equation turbulence models considered below use the Boussinesq approximation to model the Reynolds stress tensor using an eddy viscosity:

$$R_{ij} = -\overline{\rho u_i' u_j'} = \nu_t \left(\frac{\partial \bar{u}_i}{\partial x_j} + \frac{\partial \bar{u}_j}{\partial x_i} \right) - \frac{2}{3} k \delta_{ij} \tag{4}$$

2.1.1 Standard $k-\epsilon$ Model

In standard $k-\epsilon$ model [23] the turbulent kinetic energy and its dissipation rate equations can be written as follows:

$$\frac{\partial \rho k}{\partial t} + \frac{\partial}{\partial x_j} (\rho \bar{u}_j k) = \frac{\partial}{\partial x_j} \left[\frac{\left(\mu + \frac{\mu_t}{\sigma_k} \right) \partial k}{\partial x_j} \right] + P - \rho \epsilon \tag{5}$$

$$\frac{\partial \rho \epsilon}{\partial t} + \frac{\partial}{\partial x_j} (\rho \bar{u}_j \epsilon) = \frac{\partial}{\partial x_j} \left[\left(\mu + \frac{\mu_t}{\sigma_\epsilon} \right) \frac{\partial \epsilon}{\partial x_j} \right] +$$

$$\frac{\epsilon}{k(C_{\epsilon 1} P - C_{\epsilon 2} \rho \epsilon)} \tag{6}$$

Where $\mu_t = \frac{\rho C_\mu k^2}{\epsilon}$ is the eddy viscosity and P the production of the turbulent energy. For incompressible flow, P is written as:

$$P = -\frac{\overline{\rho u_i' u_j'} (\partial \bar{u}_i)}{\partial x_j} = \frac{\mu_t \left(\frac{\partial \bar{u}_i}{\partial x_j} + \frac{\partial \bar{u}_j}{\partial x_i} \right) (\partial \bar{u}_i)}{\partial x_j} \tag{7}$$

The model constants are given by:

$$C_\mu = 0.09, \quad \sigma_k = 1.0, \quad \sigma_\epsilon = 1.3, \\ C_{\epsilon 1} = 1.44, \quad C_{\epsilon 2} = 1.92.$$

2.1.2 LRN $k-\epsilon$ model:

The equations of the Low-Reynolds Number $k-\epsilon$ models [17] tested in the present work have been defined as follows:

$$\frac{\partial \rho k}{\partial t} + \frac{\partial}{\partial x_k} (\rho \bar{u}_k k) = \frac{\partial}{\partial x_j} \left[\frac{\left(\mu + \frac{\mu_t}{\sigma_k} \right) \partial k}{\partial x_j} \right] + P - \rho \epsilon \tag{8}$$

$$\frac{\partial \rho \epsilon}{\partial t} + \frac{\partial}{\partial x_k} (\rho \bar{u}_k \epsilon) = \frac{\partial}{\partial x_j} \left[\left(\mu + \frac{\mu_t}{\sigma_\epsilon} \right) \frac{\partial \epsilon}{\partial x_j} \right] +$$

$$\frac{\epsilon}{k(f_1 C_1 P - \rho f_2 C_2 \epsilon)} \tag{9}$$

Where μ_t is the eddy viscosity defined by:

$$\mu_t = \rho C_\mu f_\mu k^2 / \epsilon \tag{10}$$

The values of damping functions, wall boundary conditions and various constant for low-Reynolds number $k-\epsilon$ model are given in table 2.

Table 2: Damping functions and wall boundary condition for low-Reynolds number $k-\epsilon$ model

| f_1 | f_2 | f_μ | ϵ_W (Wall BC) |
|-------|-------|---------|------------------------|
| (5) | | | |

| | | | |
|---|---------------------------|---------------------------------------------------------|------------------|
| 1 | $(1 - 0.3 \exp(-Re_T^2))$ | $\exp\left(-\frac{3.4}{(1 + \frac{Re_T}{50})^2}\right)$ | $\epsilon_W = 0$ |
|---|---------------------------|---------------------------------------------------------|------------------|

2.1.3 $k - \omega$ SST model:

The shear-stress transport (SST) $k - \omega$ model was developed by Menter [10] to effectively blend the robust and accurate formulation of the $k - \omega$ model in the near-wall region with the free stream independence of the $k - \epsilon$ model in the far field.

The SST $k - \omega$ model has a similar form to the standard $k - \omega$ model:

$$\frac{\partial \rho k}{\partial t} + \frac{\partial}{\partial x_j} (\rho \bar{u}_j k) = \frac{\partial}{\partial x_j} \left[\frac{(\mu + \frac{\mu_t}{\sigma_k}) \partial k}{\partial x_j} \right] + G_k - Y_k + S_k \quad (11)$$

$$\frac{\partial \rho \omega}{\partial t} + \frac{\partial}{\partial x_j} (\rho \bar{u}_j \omega) = \frac{\partial}{\partial x_j} \left[\frac{(\mu + \frac{\mu_t}{\sigma_\omega}) \partial \omega}{\partial x_j} \right] + G_\omega - Y_\omega + S_\omega \quad (12)$$

In these equations, G_k represents the generation of turbulence kinetic energy due to mean velocity gradients. G_ω represents the generation of ω .

Where σ_k and σ_ω are the turbulent Prandtl numbers for k and ω , respectively and μ_t , the eddy viscosity.

2.1.4 Blended LRN $k - \epsilon$ Model (BLM)

The basic idea of this model is combination of an accurate formulation [16] of the LRN $k - \epsilon$ model and robustness of the standard $k - \epsilon$ model to reduce the sensitivity to free stream (in the outer part of the boundary-layer and in free-shear flows). The turbulent viscosity of the new model is obtained by multiplying the turbulent viscosity of LRN $k - \epsilon$ model by a function $(1 - F_b)$ and adding the results of standard $k - \epsilon$ model with a function F_b . F_b

is a blending function which ensures that the model behaves as a (standard $k - \epsilon$ model) High-Re $k - \epsilon$ model away from the surface and as the LRN $k - \epsilon$ model in the near-wall region. If μ_{t1} represents the eddy viscosity in the LRN $k - \epsilon$ model, μ_{t2} represent the eddy viscosity in the standard $k - \epsilon$ model and μ_t the eddy viscosity of the new model, the μ_t relation can be written as:

$$\mu_t = (1 - F_b)\mu_{t1} + F_b\mu_{t2} \quad (13)$$

The blending function $[(F)_b]$ is selected to ensure asymptotic consistency with the near-wall behavior of the equation of motion. The value of function F_b will be designed to be zero in the near-wall region (activating the LRN $k - \epsilon$ model) and set to unity away from the surface (switching to the High-Re $k - \epsilon$ model).

For the present model, the blending function from the LRN two-equation model of Abe et al. [7] has been tentatively adopted.

$$F_b = \left(1 - e^{-\left(\frac{y^*}{14}\right)^2}\right)^2 \left(1 + 5Re_T^{-0.75} e^{-\left(\frac{Re_T}{200}\right)^2}\right) \quad (14)$$

$$\text{Where; } y^* = \frac{(v\epsilon k)^{0.25} y}{\nu} \text{ and } Re_T = \frac{\rho k}{\epsilon \mu}$$

2.1.5 Mixed Eddy Viscosity Model (MEVM)

We need to find a type of mixed eddy viscosity formulation inspired from the formulation of the mixed scales model proposed by Sagaut [24] for the subgrid viscosity. We take this formulation in order to express the eddy viscosity as a weighted geometric mean of two linear expressions:

$$\mu_t = \mu_{LRNKE}^\alpha \mu_{SKE}^{1-\alpha} \quad (15)$$

Where μ_{LRNKE} and μ_{SKE} is the eddy viscosity of LRN $k - \epsilon$ model (eq. 10) and standard $k - \epsilon$ model respectively. We found the standard $k - \epsilon$ model for $\alpha = 0$ and the LRN $k - \epsilon$ for $\alpha = 1$, we obtain the mixed eddy

viscosity model for $\alpha = 0.5$ because of its good agreement with experimental data. In table 3, an overview of the used turbulence models are presented.

Table 3: Overview of the used turbulence models

| Turbulence model designation | Short cut | Remark |
|-----------------------------------------------------------|-----------|-------------------------------|
| Standard or High Reynolds Number $k-\epsilon$ Model | SKE | Standard model in Fluent |
| LRN $k-\epsilon$ model | LRN | In Fluent implemented via UDF |
| Blended LRN $k-\epsilon$ Model | BLM | In Fluent implemented via UDF |
| $k-\omega$ SST model | SST | Standard model in Fluent |
| Mixed Eddy Viscosity Model | MEVM | In Fluent implemented via UDF |
| Linear Pressure Strain version of Reynolds stresses Model | RSM, LPS | Standard model in Fluent |

3. Numerical procedure

The finite volume method [25], adopted in this study, express results of the study size (mass, energy, quantity of movement) on a control volume and the Gauss's law is used to transform volume integrals to surface integrals. To locate the different variables, we use the concept of interlaced mesh where pressure, turbulent kinetic energy, dissipation, the Reynolds stresses are treated at the center of the control volumes, velocity are measured at the center of the faces and the shear tensions are located at the corners. The advection terms are evaluated using the First Order Upwind scheme. The algorithm involves calculating a steady flow reducing to unsteady terms of conservation equations. In this study, we use a Semi-Implicit Method for Pressure-Linked Equations (SIMPLE) algorithm which is to express the velocity $\bar{u}_i^{(n+1)}$ at time $(n+1)\Delta t$ function of $P^{(n+1)}$ from the equations of conservation. We then obtain a Poisson

equation to solve for the pressure $P^{(n+1)}$ and combining with the equation of conservation of momentum, we obtain a new velocity field at the time $(n+1)\Delta t$ satisfying the equation of mass conservation. The inlet is modeled as velocity inlet because the flow is incompressible. Pressure outlet conditions are imposed at the outlet with zero gauge pressure. This is acceptable since, for incompressible flows, the pressure gradient is the necessary information in solving the Navier-Stokes equations instead of absolute pressures itself. All the remaining surfaces except symmetry are imposed with no-slip at wall boundary conditions.

4. Results and Discussion

The present test cases are selected on the important criterion that the near-wall and low-Reynolds number effects need to be solved. Evidence of acceptable agreement with the available experimental or DNS are expected. In the present work, calculations have been performed for the following test cases: Flow past backward-facing step by Jovic et al. [18] and Flow over repeated square ribs by Drain and Martin [25].

4.1 Flow past backward-facing step

The flow over a backward-facing step has the most basic features of separated flows, such as separation, reattachment, recirculation, and development of shear layers. It is typically considered as a suitable test case for turbulence model validation. The ability of the proposed model is shown through simulations for double-sided backward-facing step flows at $Re_h = 5000$ by Jovic et al. [18]. The backward-facing step configuration is symmetric about the centerline of the channel. Thus, only half of the channel is employed as the computational domain. A schematic sketch of the experimental set up is shown in Figure 1. It runs from $-10h$ to $30h$, where h is the height of the step. The height of the input stream is $5h$. In the present case, the control parameters of the flow are the Reynolds number based on the height of the step Re_h and the expansion ratio (ER) defined by:

$$Re_h = \frac{hU_o}{\nu}, ER = \frac{Ly}{(Ly - h)} \tag{16}$$

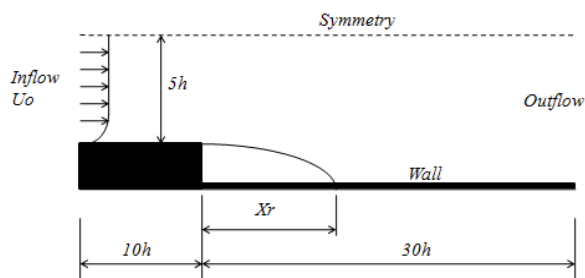


Fig. 1: Schematic diagram of experiment and boundary conditions

At the entrance of the computational domain, we imposed a velocity profile corresponding to power law on mean velocity U.

$$\frac{U}{U_o} = \left(\frac{y}{R}\right)^{\frac{1}{n}} \tag{17}$$

where $n=7$ and $U_o = 44.2 \frac{m}{s}$.

The other velocity components are initialised to zero in the whole area. The computational grid for this geometry is meshed with quadrilateral elements to minimize the numerical errors. Here the objective is to predict the reattachment point, fine meshes are placed around the step and near walls to resolve the high gradients encountered in these regions. Moreover, grids are generated by Gambit software [20] to discretize the physical domain.

In CFD simulations, the mesh should be fine enough to capture the flow gradients and also to reduce the numerical errors. In general, this is achieved by meshing with different number of grid elements and observing the change in a certain quantity of interest. The reattachment length is the most crucial single quantity in this study and is used to study the grid independence for the backward-facing step test case.

Three different grids are meshed with different grid spacing and simulated with SKE turbulence model. All of the other variables are kept unchanged. Table 3 shows the results of this study with non-dimensional reattachment

length, $\frac{X_r}{h}$, for different number of grid elements.

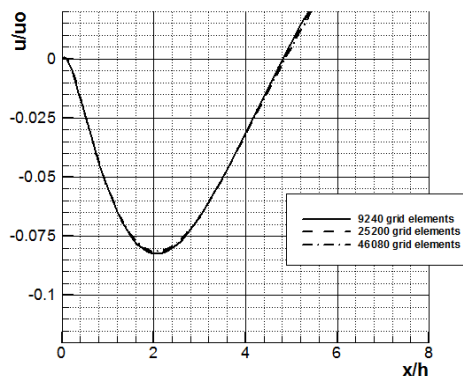


Fig. 2: Number of grid elements sensitivity

It can be observed that 25200 grid elements are sufficient enough to represent the flow (Fig. 2). Employing 40680 elements increase the computational cost without much advantage. For the rest of the study, mesh with 9240 elements is used.

The pressure coefficient on the wall (C_p) on the channel floor is computed and compared with the experimental results of Jovic et al. [18] and also with DNS simulations of Le et al. [28] (Fig.3) to characterize the flow separation and reattachment. The pressure coefficient is defined as

$$C_p = \frac{P - P_o}{\frac{1}{2} \rho U_{ref}^2} \tag{18}$$

(18)

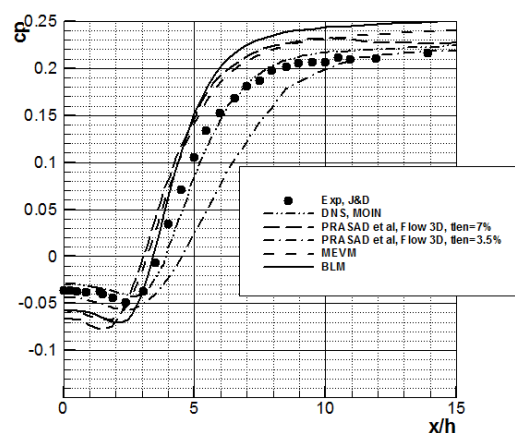


Fig. 3: Coefficient of pressure (C_p), along the channel floor

Figure 3 presents the pressure coefficient on the downstream wall of the step. The analysis of this curve decomposes the flow into three distinct zones: a zone of recirculation, a zone of reattachment and a zone of back into balance. In the recirculation zone, the peak pressure coefficient is over-estimated both by the RNG k-ε model of Prasad et al [27], by the BLM and MEVM models. This result can be attributed to the use of wall laws. The reattachment zone is characterized by a rapid increase of the pressure coefficient due to compression at the reattachment. The slope of the curve of the coefficient of pressure is correctly predicted by BLM and MEVM models. The area of return to equilibrium of boundary layer is characterized by a pressure coefficient constant value overestimated by different models.

In the present case, the streamwise velocity in the first cell above the wall is extracted to check the point where $u = 0$. A similar shift in profile is observed in the streamwise velocity along the channel for the first cell just above the wall. Reattachment length X_r is taken as the point where the streamwise velocity $u = 0$ for the first cell above the wall. See Figure 4.

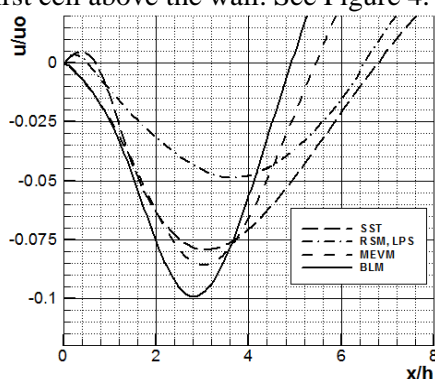


Fig. 4: Streamwise velocity along the channel floor to measure the reattachment length

The position of the reattachment point is an important parameter that has often been used to compare the performance of turbulence models.

Table 4: Sensitivity of reattachment length for different grids

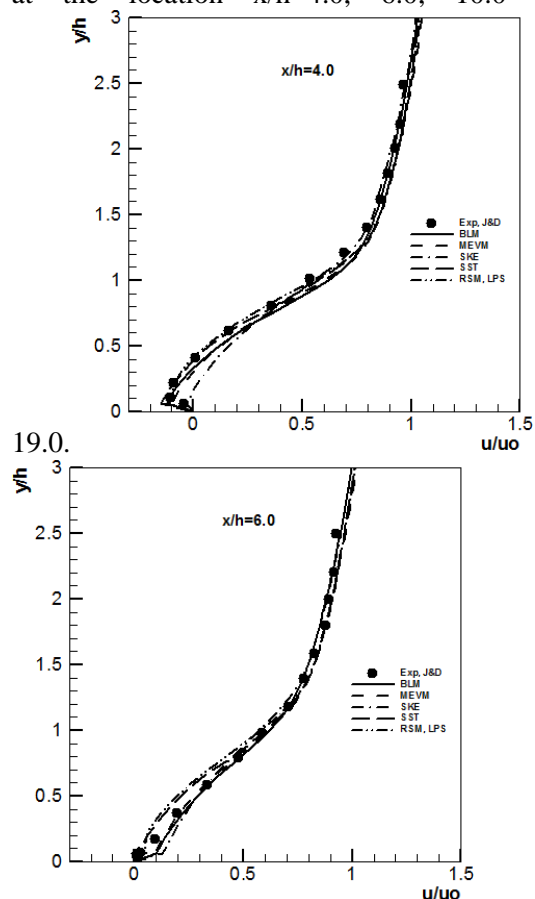
| Case | Number of Grid elements | $\frac{X_r}{h}$ |
|------|-------------------------|-----------------|
| 1 | 9240 | 4.809 |
| 2 | 25200 | 4.856 |
| 3 | 40680 | 4.888 |

In Table 4, we compare the reattachment length calculated with different models and experimental data. According to Jovic and Driver [18], the reattachment length ($\frac{X_r}{h}$) is between 6.0 and 6.1. The DNS performed by Le et al [28] predicts a value equal to 6.28. For the present work, table 4 provides the values of 5.4538 and 4.9194 respectively for MEVM model and BLM model.

Table 5: Sensitivity of the reattachment length to the turbulence model

| Turbulence Models | $\frac{X_r}{h}$ | %ERR |
|-------------------|-----------------|-------|
| MEVM | 5.4538 | 9.4 |
| k-ω SST | 6.0982 | 1.6 |
| RSM LPS | 5.9567 | 0.7 |
| BLM | 4.9194 | 18.01 |

For the normalized mean velocity, the proposed models show reasonable agreement with experimental data. Figure 5 shows model comparisons of the mean streamwise velocity normalized by the reference flow velocity (u_o) at the location $x/h=4.0, 6.0, 10.0$ and



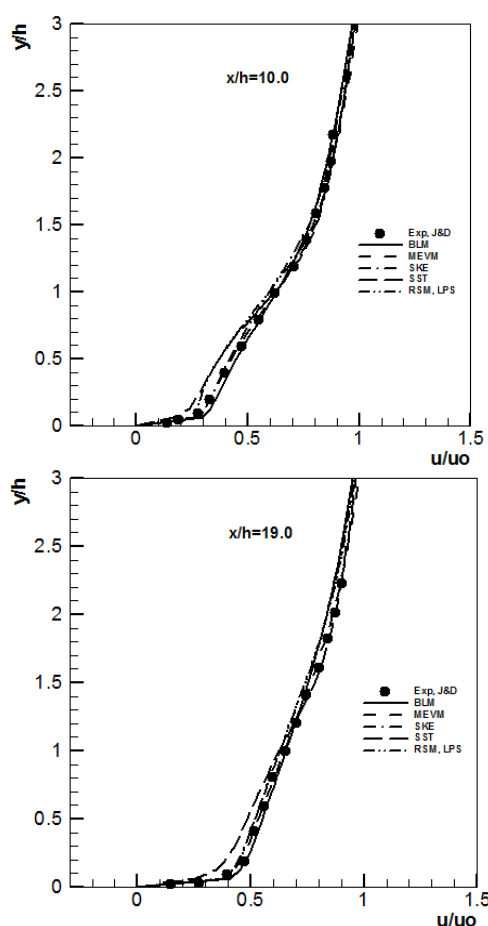


Fig. 5: Normalized mean stream wise

velocities ($\frac{u}{U_o}$) at the location $x/h= 4.0; 6.0; 10.0; 19.0$

4.2 Flow over repeated square ribs

The final test case is the flow over repeated square ribs. The turbulent channel flows containing rib-roughened walls have been extensively studied for many years, owing to broad applicability across numerous engineering applications. Although similar to a combined backward-facing step [18] and forward-facing step [29], the turbulent flow field generated from a rib is more complex resulting from the separation of both rib edges. In addition, the presence of successive ribs provides another layer of complexity resulting from interactions between the rib-induced wakes. A computational study by Cui et al. [30], using a Large Eddy Simulation (LES), to investigate the results of various pitch-to-height ratios in a two-dimensional channel with ribs. Repeated studies were indicated by Miyake et al. [31], Ikeda and Durbin using DNS [32] and Ryu et al. [33] using the $LRN k - \omega$ model.

More recently, Khuwaranyu et al. [16] proposed a concept for a new turbulence model, which combines the $LRN k - \omega$ model with a Length Scale Correction (LSC) term and applied it to the problem of recirculating flow over repeated square ribs.

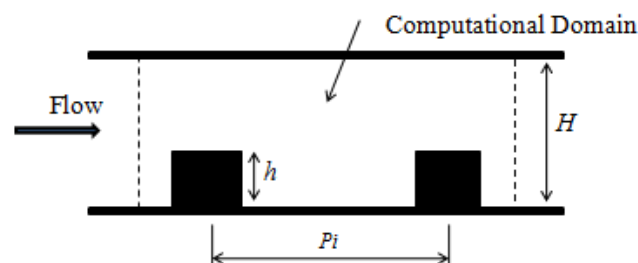


Fig. 6: Computational domain and Repeated square ribs configuration

For the current study, the experimental data from Drain and Martin (1985) are used for validating flow over a smooth wall with square sectioned ribs. The spanwise square ribs are mounted on the bottom wall of a channel as shown in Figure 6. The Reynolds number ($Re_{De} = 37,200$) is calculated with respect to the bulk velocity (U_b) and the hydraulic diameter (H). To solve the near-wall flow problem, fine-grid spacing is applied in the region next to channel walls and rib surfaces. Dimensions of the test case are given as follows: the size of each rib is 8×8 mm, the

pitch-to-height ratio ($\frac{Pi}{h}$) is 7.2 and the channel-

to-rib height ratio ($\frac{H}{h}$) is 5.0. The inlet and outlet sections are prescribed with periodic boundary conditions. The normalized streamwise velocity profiles at different

locations ($\frac{x}{h} = 0.0, 3.68, 4.82, 6.80$) are presented in Figure 7.

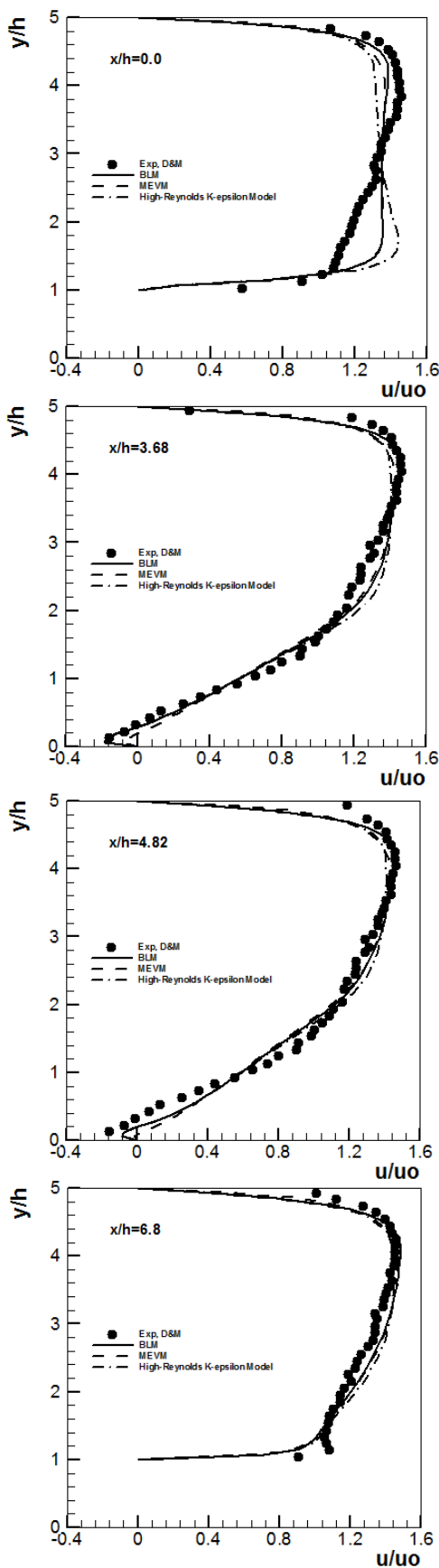


Fig. 7: Normalized mean stream wise velocities ($\frac{u}{U_o}$) at the location $x/h= 0.0; 3.68; 4.82; 6.8$

It can be seen that the numerical results are in satisfactory agreement with the experimental data of Drain and Martin (1985) in all regions. Some discrepancies are found in the region above rib surfaces ($\frac{x}{h} = 0.0$ and $\frac{x}{h} = 6.8$). Manceau et al. (2000) in noting these types of discrepancies suggested that the experiment probably exhibited 3-D effects such as counter rotating eddies in the x-direction located between the top surface of the ribs and upper channel wall. These effects might induce flow acceleration on the measurement plane where they converge and deceleration where they diverge. In the region between two ribs, two recirculation zones can be observed.

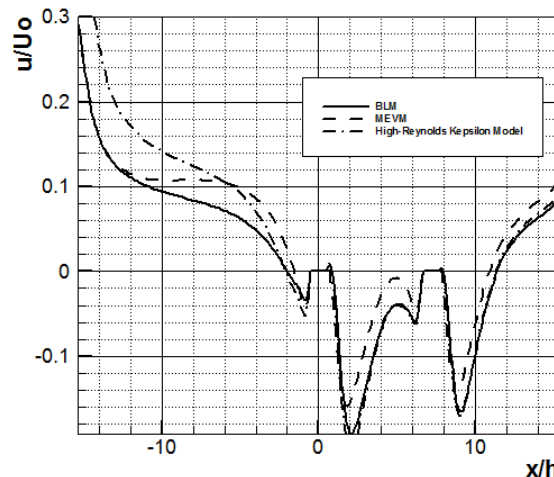


Fig. 8: Streamwise velocity along the channel floor to measure the reattachment length

The experiment reports the reattachment of the ribbed channel flow after the first rib at about $4.32h$, whereas the proposed models give the values of approximately $4.11h$ and $3.906h$ respectively for BLM and MEVM (See figure 8). Thus, the present simulation with the BLM and MEVM turbulence models indicate respectively a 4.86% and 9.01% underprediction of the reattachment length compared to experimental result.

5. Conclusion

In this study, the combined concepts of turbulence models for recirculating flows are presented. The proposed model combines LRN

k- ϵ model capacity in near wall region with the performance of standard k- ϵ model to reduce the sensitivity of the free stream. For this purpose two approaches have been proposed, BLM and MEVM. The performance of the models is validated by two well-known test cases: Backward-facing step flow and flow over repeated square ribs. Despite the existence of some discrepancies, the proposed models demonstrated their performance for accommodating the near-wall low-Reynolds number effect for turbulent recirculating flows.

Acknowledgment

The author wishes to express his gratitude to Dr. Ruben MOUANGUE, Dean of Department of Energetic Engineering of the University of Ngaoundéré for making available for us Fluent and Gambit software.

References:

1. Launder B.E, Spalding D.B (1972). "Mathematical Models to Turbulence". Academic Press London.
2. Patel V.C, Yoon J.Y (1985). "Turbulence models for near-wall and low Reynolds numbers flows" – A review. AIAA J. 23: 1308-1319.
3. Peng S.H, Davidson L, Holmberg S (1997). "A modified low-Reynolds-number $k-\omega$ model for recirculating flows". J. Fluid Eng-T. ASME 119: 867-875.
4. Jones W.P, Launder B.E (1973). "The calculation of low-Reynolds-number phenomena with a two-equation model of turbulence". Int. J. Heat Mass Tran. 16: 434-440.
5. Lam C.K, Bremhorst K (1981). "A modified form of the $k-\epsilon$ model for predicting wall turbulence". J. Fluid Eng-T. ASME 103: 456-460.
6. Chien K.Y (1982). "Predictions of channel and boundary-layer flows with a low-Reynolds-number turbulence model". AIAA J. 20: 33-38.
7. Abe K, Kondoh T, Nagano Y (1994). "A new turbulence model for predicting fluid flow and heat transfer in separating and reattaching flows- I. Flow field calculations". Int. J. Heat Mass Tran. 37: 139-151.
8. Chang K.C, Hsieh W.D, Chen C.S (1995). "A modified low-Reynolds-number turbulence model applicable to recirculating flow in pipe expansion". J. Fluid Eng-T. ASME 117: 417-423.
9. Menter F.R., (1992). "Improved two-equation $k-\omega$ turbulence models for aerodynamic flows". NASA TM-103975. NASA-Ames research center. USA: 1-31.
10. Menter F. R., (1994). "Two-Equation Eddy-Viscosity Turbulence Models for Engineering Applications", AIAA Journal, Vol. 32, pp. 1598-1605.
11. Bredberg, J., Davidson, L., (2004). "Low-Reynolds Number Turbulence Models: An Approach for Reducing Mesh Sensitivity," ASME Journal of Fluids Engineering, Vol. 126, pp 14-21.
12. Wang S.J, Mujumdar A.S (2005). "A comparative study of five low Reynolds number $k-\epsilon$ models for impingement heat transfer". Appl. Therm. Eng. 25: 31-34.
13. Yap C.J., (1987). "Turbulent heat and Momentum Transfer in Recirculating and Impinging Flows". Ph. D. Dissertation. University of Manchester.
14. Jia R, Sunden B, Faghri M., (2007). "A new low Reynolds stress transport model for heat transfer and fluid in engineering applications". J. Heat Trans Mass Tran. 16: 1119-1130.
15. Spezial C.G, Sarkar S, Gatski T.B., (1991). "Modelling the pressure-strain correlation of

turbulence: an invariant dynamical systems approach". J. Fluid. Mech. 227: 245-272.

16. Khuwaranyu K, Putivisutisak, S., (2009). "Combined low-Reynolds-number $k-\omega$ model with length scale correction term for recirculating flows" J. Eng. Technol. Res. Vol. 1 (8), pp. 171-180.

17. Abid R., (1993). "Evaluation of two-equation turbulence models for predicting transitional flows". Int. J. Eng. Sci. 31: 831-840.

18. S. Jovic, D. Driver., (1994). "Backward-facing step measurements at low Reynolds $Re_h = 5100$

number, , "NASA Ames Research Center.

19. Hattori, H., Nagano, Y., (2010). "Investigation of turbulent boundary layer over forward-facing step via direct numerical simulation". International Journal of Heat and Fluid Flow 31, 284-294.

20. Fluent v6.3.26 Documentation (2006): User's Guide. Fluent. Inc.

21. Mansour, N. N., Kim, J., Moin, P., (1983). "Computation of Turbulent Flows over a Backward-Facing Step" NASA TM-85851.

22. M. Popovac., (2010). "Robust eddy viscosity turbulence modeling with elliptic relaxation for external building flow analysis," Fourth National Conference of IBPSA-USA, New-York, August 11-13.

23. B.E. Launder and D.B. Spalding., (1974). "The numerical computation of turbulent flow. Comput," Methods Appl. Mech. Eng., 3; 269.

24. Sagaut P., (1996). "Numerical simulations of separated flows with subgrid models, Rech. Aéro. 1: 51-63.

25. S. V. Patankar., (1980). "Numerical heat transfert and fluid flow," Hemisphere. Washington, D, C. pp 115-120.

26. Drain L.E, Martin S., (1985). "Two-component velocity measurements of turbulent flow in a ribbed-wall flow channel. International Conference on Laser Anemometry-Advances and Applications. UK.

27. Prasad V. Tota., (2009). "Turbulent Flow over a Backward-Facing Step Using the RNG $k-\epsilon$ Model," Flow Science, Inc. FSI-09-TN81.

28. Hung, Le, Moin, P., and Kim, J., (1980). "Direct numerical simulation turbulent shear layer: flow over a backward facing step," ASME J. Fluids. Eng, Vol. 102, pp 302-308.

29. Hattori H and Nagano Y., (2010). "Investigation of turbulent boundary layer over forward-facing step via direct numerical simulation" International Journal of Heat and Fluid Flow 31, 284-294.

30. Cui J, Patel V. C, Lin C. L., (2003). "Large-eddy simulation of turbulent flow in a channel with rib roughness. Int. J. Heat Fluid Fl. 24: 372-388.

31. Miyake Y, Tsujimoto K, Nagai N., (2002). "Numerical simulation of channel flow with a rib-roughened wall". J. Turbul. 3: 1-17.

32. Ikeda T, Durbin P. A., (2002). "Direct simulations of a rough-wall channel flow". Mechanical engineering Report TF-81. Stanford University. UK.

33. Ryu D. N, Choi D. H, Patel V. C., (2007). "Analysis of turbulent flow in channels roughened by two-dimensional ribs and three-dimensional blocks, Part I: Resistance. Int. J. Heat Fluid Fl. 28: 1098-1111.

